




Particle manipulation based on the controllable light field of graphene nano-butterfly structures

Jinfeng Li ^a, Jinyang Gong ^b, Zhihao Li ^a, Xiaoling Li ^a, Min Jiang ^b  


[Show more](#) 

 [Outline](#) |  [Share](#)  [Cite](#)

<https://doi.org/10.1016/j.optcom.2024.130911> 

[Get rights and content](#) 

Under a Creative Commons [license](#) 

 [open access](#)

Highlights

- An optical conveyor belt based on the periodically arranged graphene nano-butterfly structures is proposed.
- The mechanism relies on the tunable surface plasmon resonance via manipulating Fermi energy of graphene.
- The feasibility of the particle separation is demonstrated.

Abstract

In this Letter, we have proposed a nano-optical convey belt consisting of three sets of graphene nano-butterfly structures (GNBS) with different lengths arranged in a periodic

pattern to trap, transport, and sort particles depending on controlling the Fermi level of graphene. The graphene nano-butterfly structure, based on a couple of trapezoids, can form a potential well to capture particles by localized surface plasmon resonance under the excitation of an incident laser. There are three adjustable geometric parameters containing width (W_1 , W_2) and length (L) that make the GNBS have a high degree of design flexibility. Graphene can support surface plasmons in the mid-infrared region, and at the same time, it possesses a more flexible tuning mechanism compared to metals. When the incident light power is $1 \text{ mW}/\mu\text{m}^2$ and the resonance wavelength is $10.6 \mu\text{m}$, the depth of the potential well is greater than $10K_bT$ for 50 nm particles. Moreover, the sorting of particles with different diameters has also been validated under appropriate power and switching time. Based on the capabilities of capture and sorting verified by numerical analysis, our design offers a new scheme for on-chip optofluidic applications.



Previous

Next



Keywords

Nano-photonics; Photonic crystals; Metasurfaces; Plasmonic-assisted tweezers; Nanoparticle capture and sort

1. Introduction

Optical tweezers have sparked widespread discussion since Arthur Ashkin first used a highly focused laser beam as a method for trapping dielectric particles [1]. Conventional optical tweezers have a shortcoming in that the diffraction limit results in a focus that is too large to capture nanoscale particles. However, increasing the power to trap nanoparticles can result in damage to the sample [2]. Compared with conventional ones, plasmonic-assisted tweezers have been an effective technique for trapping and manipulating particles [3]. Plasmonic-assisted tweezers can generate stronger optical gradient force by plasmon resonance on the surface of metallic material to realize higher precision and efficiency in manipulating small objects. In recent years, many designs based on plasmon-assisted optical tweezers have been reported, which can trap particles by forming hot spots with low power density [[4], [5], [6]]. Wang et al. first proposed that particles with a diameter as small as 110 nm can be captured by gold nano-disks and the team demonstrated the capture of micrometer-scale fluorescent beads by surface plasmon resonance [7,8]. TD Bouloumis et al. captured 20 nm gold particles using the combined effects of SIBA and Fano resonance in

metamaterial tweezers [9]. DG Kotsifaki et al. designed asymmetric split-ring plasmonic nanostructures based on Fano resonance to identify and detect Escherichia coli [10]. Additionally, Shiho Tokonami et al. proposed a laser-induced assembly method for a honeycomb substrate to achieve high-density cell assembly [11].

Although the current work has completed the capture of particles, there is a huge challenge for one-dimensional long-distance transportation and arbitrary manipulation of two-dimensional. Hansen et al. proposed an optical conveyer belt with C-shape apertures to sort nano-particles by controlling resonant wavelengths and polarizations [12,13]. Moreover, nano-particles can achieve 2D arbitrary manipulation on a plasmonic nano-ellipse metasurface, as reported by Jiang [14]. While the above-mentioned research has made certain progress, the plasmon resonance on the metallic surface requires the modulation of resonance wavelengths and polarization, which increases the complexity of the system owing to the precise tuning and high-level coordination.

Graphene is a two-dimensional material formed by carbon atoms arranged in a pattern that resembles a hexagonal honeycomb. Since the successful isolation of single-layer graphene in 2004, graphene has garnered significant interest within the scientific and industrial communities because of its exceptional physical, chemical, and electrical characteristics [15, 16]. In recent years, besides single-layer graphene, two-dimensional materials such as black phosphorus, MXene, and graphene oxide have also been widely used in various metasurface designs [[17], [18], [19]]. Compared with the metal plasmon, many nanostructure designs based on the graphene plasmon have proved that it can greatly enhance field confinement to achieve larger optical gradient forces. Graphene possesses exceptionally high thermal conductivity, which can further reduce the thermal damage to captured samples by optical tweezers and improve the stability of the transmission process [20]. Additionally, graphene can modulate the distribution of carrier density, thereby controlling surface conductivity [21]. This method of manipulation could serve as an alternative to adjusting the wavelength and polarization which can further reduce the difficulty of operating the entire system [[22], [23], [24]].

In this work, we elaborate on the design concept and working principle of the optical conveyer belt based on graphene nano-butterfly nanostructures, which can trap and sort nanoparticles with different diameters. The control mechanism of the optical conveyer belt we propose is not based on wavelength and polarization, but rather on the Fermi level, which can be adjusted through electrodes. We use the three-dimensional finite-difference time-domain (FDTD) method to verify the feasibility of the nano-optical conveyer belt and

employ the Volumetric technique to calculate the optical forces exerted on the particles. Additionally, we conduct statistical analysis on the particle separation process.

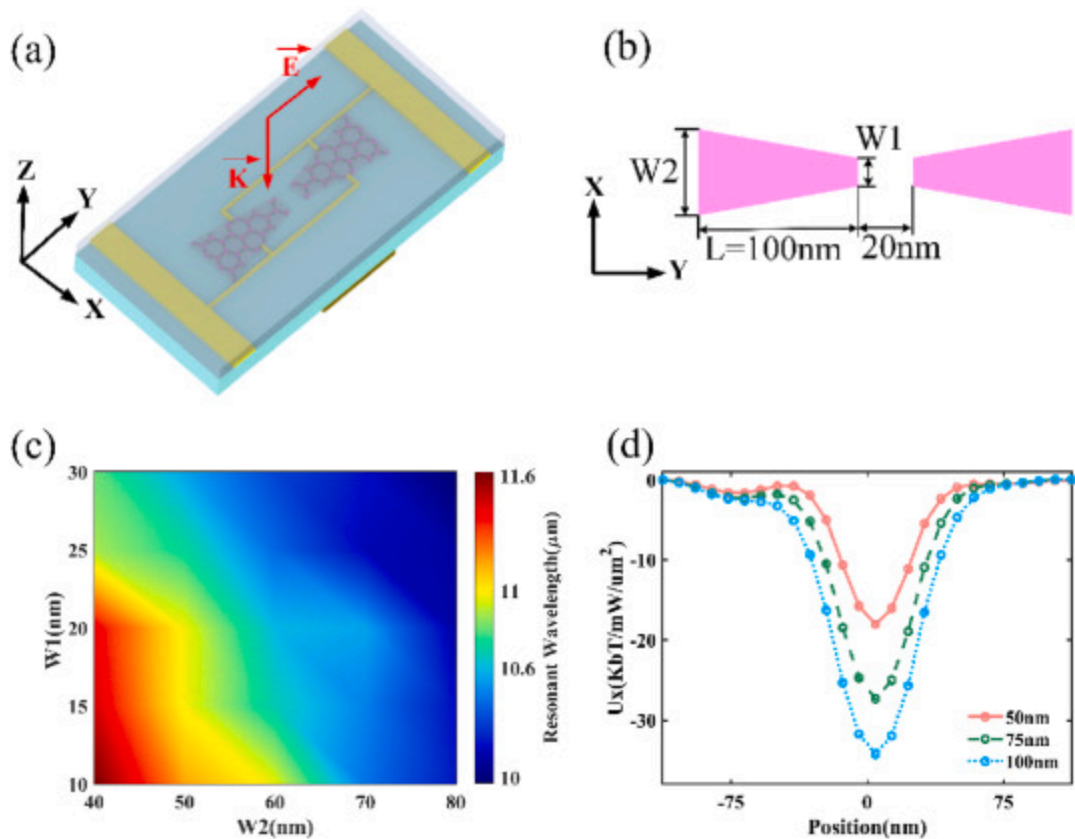
2. Graphene metasurface

First, it is necessary to verify the particle capture capability of the graphene nano-butterfly structure. The material of the graphene nano-butterfly structure is set based on an equivalent volumetric permittivity model, which can be defined by the following equation:

$$\epsilon_{xx} = \epsilon_{yy} = \epsilon_r - \frac{\mu_c e^2 \omega}{\pi \hbar^2 (\omega^2 + \tau^{-2})} \frac{1}{\omega \epsilon_0 \Delta} + i \frac{\mu_c e^2}{\pi \hbar^2 (\omega^2 + \tau^{-2}) \tau} \frac{1}{\omega \epsilon_0 \Delta} \quad (1)$$

where Δ is the thickness of the graphene nano-butterfly structure, the background relative permittivity $\epsilon_r=2.5$, ϵ_0 is the vacuum permittivity, the relaxation time $\tau = \mu \mu_c / e v_f^2$, μ_c is the Fermi energy level, the carrier mobility $\mu=1 \text{ m}^2/\text{V/s}$, the Fermi velocity $v_f=1 \times 10^6 \text{ m/s}$.

As shown in Fig. 1(a), the graphene nano-butterfly structure, which is linked by gold electrodes on both sides and manipulated the Fermi energy by the gate electrode, is laid on a dielectric substrate, covered with a 10nm thick encapsulation layer ($n=1.45$), and the whole assembly is placed in a liquid environment ($n=1.33$). Fig. 1(b) shows the graphene nano-butterfly structure consisting of a pair of trapezoidal structures spaced 20nm apart, with adjustable lengths (L) and widths ($W1, W2$). We discussed the impact of variations in width $W1$ and $W2$ on the resonance wavelength of the graphene nano-butterfly structure when the Fermi level is 0.67 eV and the length is 100nm in Fig. 1(c). The resonance wavelength can be tuned within a certain range and reaches its maximum as the width decreases. Furthermore, when $W1$ is 20nm and $W2$ is 60nm with a resonant wavelength of 10.6 μm , Fig. 1(d) demonstrates the depth of potential well for 50nm particles($n=1.59$) which are located 10nm above the encapsulation layer is still greater than 10 $K_b T$.

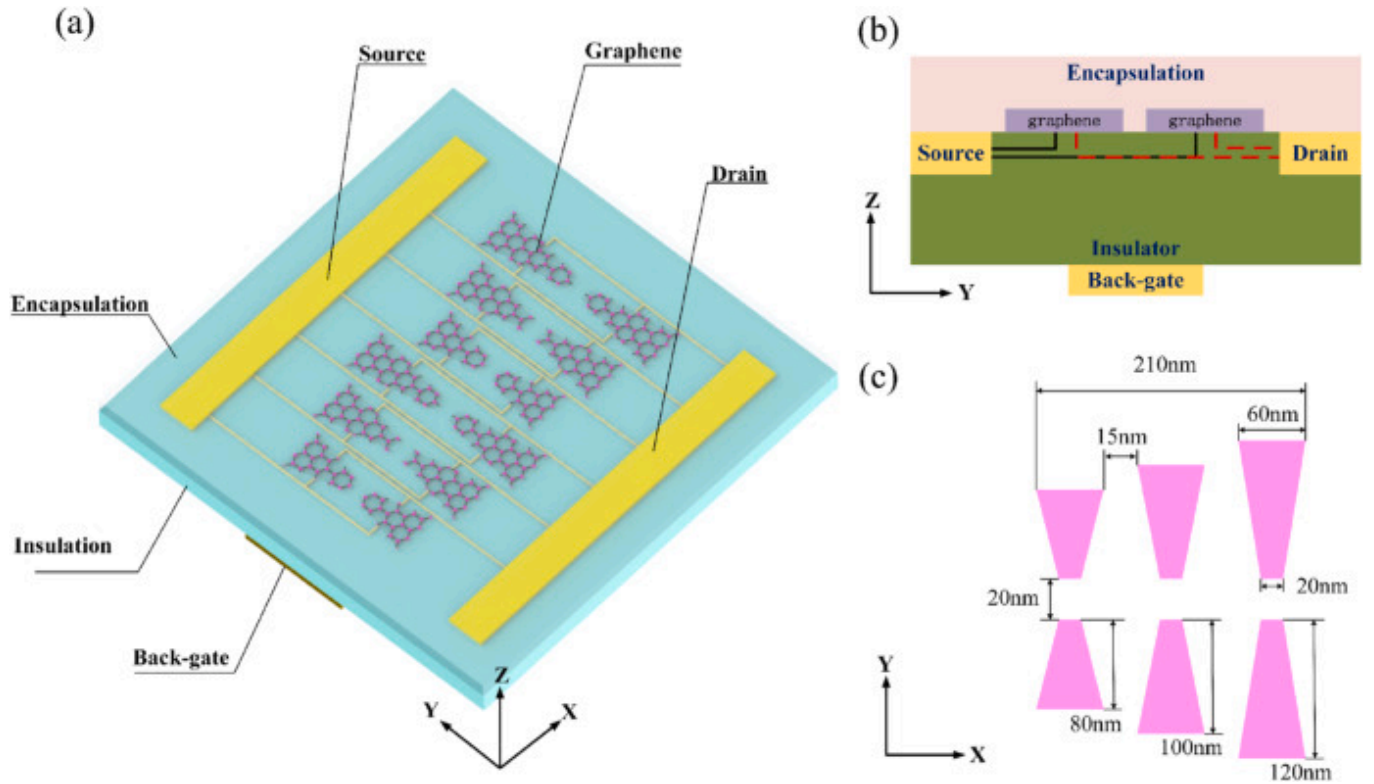


[Download: Download high-res image \(482KB\)](#)

[Download: Download full-size image](#)

Fig. 1. (a) Stereoscopic schematic of the graphene nano-butterfly structures(GNBS). (b) Structure parameters of widths($W1$, $W2$) and lengths(L) in X–Y view of the GNBS. (c) The impact of changes in $W1$ and $W2$ on the resonant wavelength when the Fermi level is 0.67eV and the length is 100nm . (d) Calculation of the potential well for polystyrene sphere ($n=1.59$, diameters= 50nm , 75nm , and 100nm), when $W1$ is 20nm and $W2$ is 60nm with a resonant wavelength of $10.6\mu\text{m}$.

As shown in Fig. 2(a) and (b), we further propose a method to implement the nano-optical conveyor belt using a periodic array with the graphene nano-butterfly structure. Similar to what is shown in Fig. 1(a), multiple sets of graphene nano-butterfly structures of varying lengths are wedged between the dielectric and encapsulation layer, with the Fermi energy of graphene being controlled through gate electrodes. The graphene nano-butterfly structure is named “GNBS- L ” based on its length, for example, “GNBS-80”. As shown in Fig. 2(c), the length of GNBSs increases incrementally from 80nm to 120nm in steps of 20nm , with widths $W1$ and $W2$ uniformly set at 20nm and 60nm , respectively. Each period consists of three GNBSs, with a spacing of 15nm between them.



[Download: Download high-res image \(504KB\)](#)

[Download: Download full-size image](#)

Fig. 2. (a) and (b) Stereoscopic schematic of the nano-optical conveyor belt. (c) The specific structure parameters of the nano-optical conveyor belt.

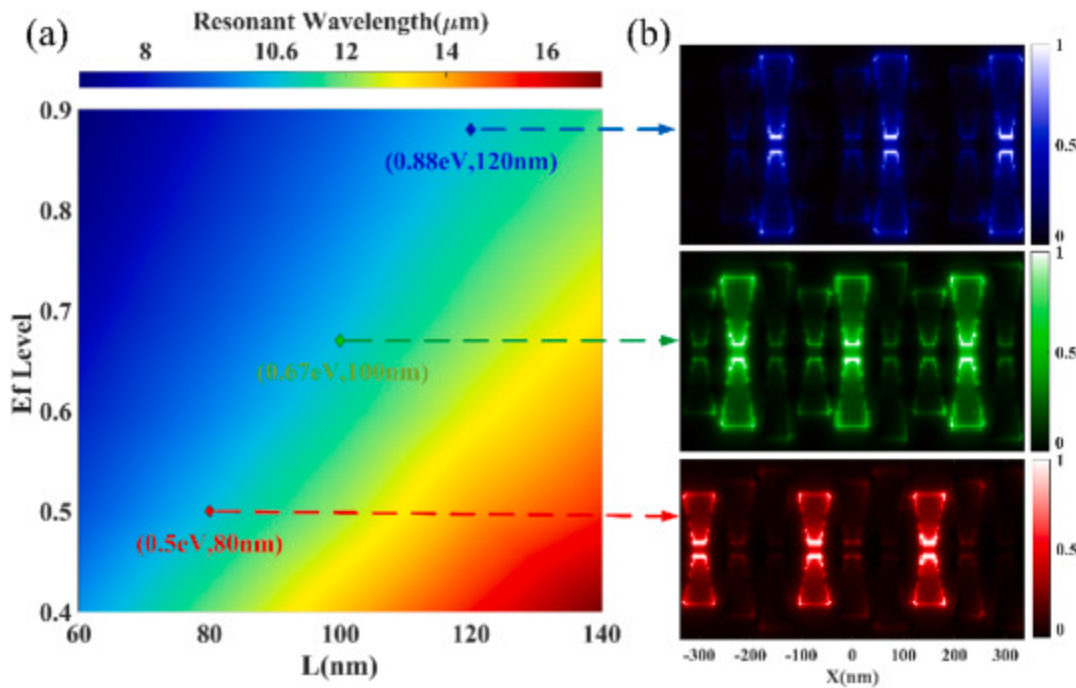
We aim to determine if localized surface plasmon resonance can selectively enhance the light field (hot spots) when a perpendicular Y-polarized beam excites the GNBS, as we manipulate the Fermi energy. Compared to metallic meta-surfaces, graphene meta-surface structures can manipulate the Fermi level to adjust the resonance wavelength. The intensity of the optical field caused by localized surface plasmon resonance can be calculated using the following formula:

$$\frac{|E_S|^2}{|E_0|^2} = \frac{2\sqrt{\epsilon_2'}(-\epsilon_2' - \epsilon_1)}{\sqrt{\epsilon_1}\epsilon_2''} \quad (2)$$

where ϵ_1 represents the dielectric constant of the environment, ϵ_2' denotes the real part of the metal complex dielectric constant and can be adjusted by controlling the number of free electrons in graphene through electrostatic gating, and ϵ_2'' is the imaginary part of the metal complex dielectric constant. In the simulation, the device is perpendicularly illuminated by a plane wave source from the top. The periodic structure is modeled using a unit cell model bounded by periodic boundary conditions to the x direction, while the perfectly matched

layer(PML) absorbing boundary conditions were used in the y and z directions. The intensity distribution of the electric field in the X–Y plane is calculated at 2nm above the GNBSs.

Fig. 3(a) shows the corresponding Fermi energy for the selected lengths at the resonant wavelength of $10.6\mu\text{m}$ when W_1 is 20nm and W_2 is 60nm. As shown in Fig. 3(b), the hotspots for GNBS-80s, GNBS-100s, and GNBS-120s will be sequentially activated, corresponding to Fermi levels of 0.5eV, 0.67eV, and 0.88eV, respectively. The captured particles will undergo one-dimensional long-distance transport along the trajectory of the moving hotspot.



[Download: Download high-res image \(589KB\)](#)

[Download: Download full-size image](#)

Fig. 3. (a) The impact of variations in length and Fermi level on the resonance wavelength, with widths W_1 and W_2 fixed at 20nm and 60nm, respectively. (b) The distribution of the electric field in the X–Y plane when GNBSs are illuminated.

3. Particle transport and automatic sorting

Compared to the capture of particles in a single plasmonic trap, the most critical issue in particle transmission is whether they can complete the transition between two adjacent plasmonic traps. The calculation of optical force uses the Volumetric technique, and the

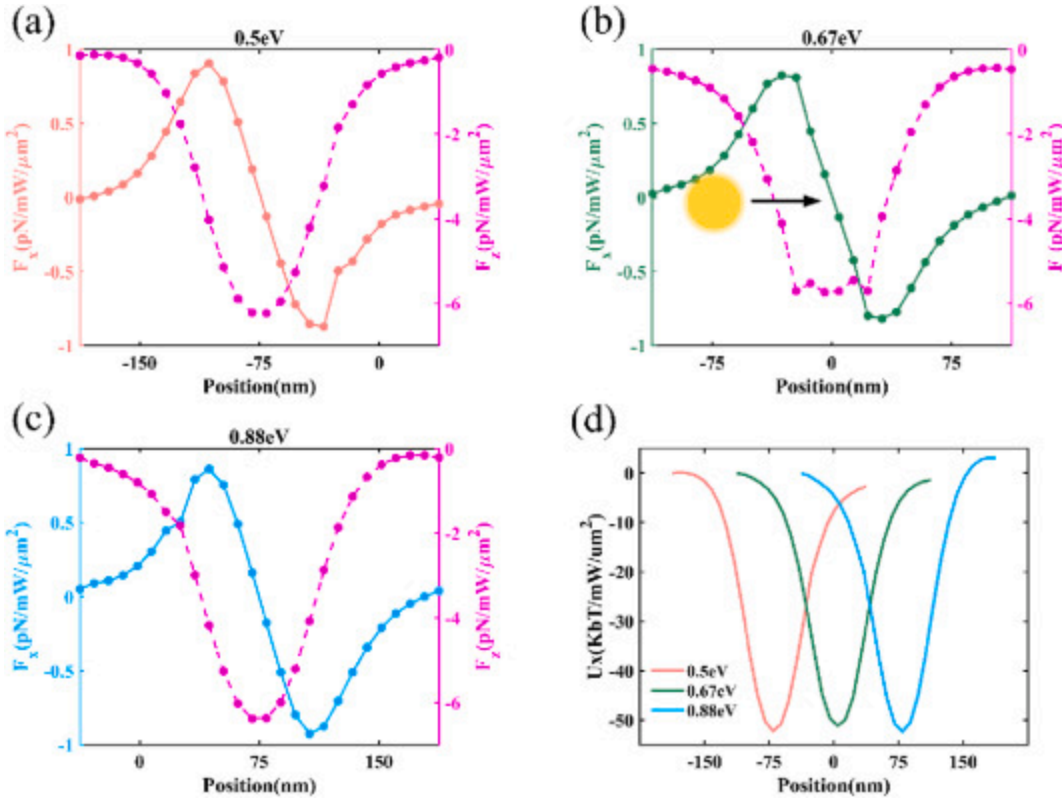
optical force per unit volume of the particle is given by the following equation:

$$\vec{F}_V = \epsilon_b \epsilon_0 \left(\vec{\nabla} \cdot \vec{E} \right) \vec{E} - i\omega \epsilon_0 (\epsilon_r - \epsilon_b) \vec{E} \times \vec{B} \quad (3)$$

where ϵ_b is the background relative permittivity, ϵ_r is the relative background permittivity throughout the volume. The potential well can be obtained by integrating the optical force calculated above, as given by the following equation:

$$U(r_0) = - \int_{\infty}^{r_0} F(r) dr \quad (4)$$

As shown in Fig. 4(a)–(c), the optical gradient force acting on a particle with a diameter of 200nm, calculated by the volumetric technique, is decomposed into horizontal component F_x and vertical component F_z . The magenta line represents F_z , which applies a force in the negative z -direction on the particle, ensuring that the particle is tightly attached to the encapsulation layer during movement. Specifically, particles already captured by the GNBS-80 will be subjected to optical forces at the pN level and will be drawn towards the GNBS-100 when the hotspot is activated and the Fermi level is 0.67 eV, as shown in Fig. 4(b). Fig. 4(d) shows the potential well depth for 200nm particles, calculated by integrating F_x when the hotspots are sequentially illuminated. The potential well depths of GNBSs with different lengths are essentially consistent and reach 50 K_bT when the incident optical power is $1 \text{ mW}/\mu\text{m}^2$.



Download: [Download high-res image \(531KB\)](#)

Download: [Download full-size image](#)

Fig. 4. The incident light power is set to $1 \text{ mW}/\mu\text{m}^2$, and the Fermi energy levels are established at 0.5 eV, 0.67 eV, and 0.88 eV. (a)–(c) The optical gradient force, as determined via the volumetric technique, is decomposed into horizontal (F_x) and vertical (F_z) components. (d) Distribution of potential wells in GNBSs of different lengths on particles with a diameter of 200 nm.

The switching time is the duration for which the hotspot is activated and sustained, and it must allow particles to complete their transition between two plasmonic traps. In practical applications, since particles are in a liquid environment, they are also subject to Brownian motion and viscous drag. Therefore, the particle motion equation is as follows:

$$m \frac{d^2 x}{dt^2} = F_{op} + F_{br} - F_{drag} \quad (5)$$

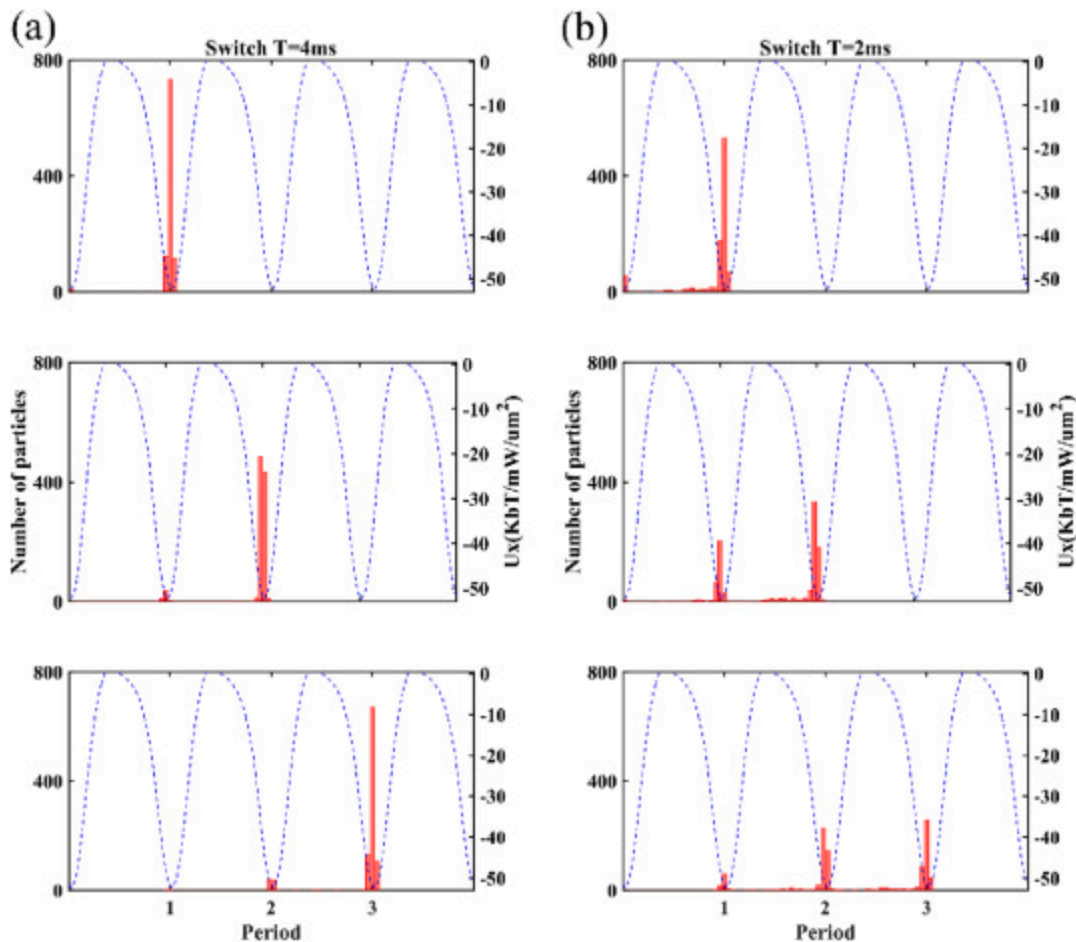
where m , x , and t represent the particle's mass, displacement, and motion time, respectively. F_{op} is the near-field optical force, and the Brownian force F_{br} and viscous drag force F_{drag} are calculated using the following equations:

$$F_{br} = R \sqrt{\left(\frac{6\pi K_b T D \gamma}{\Delta t} \right)} \quad (6)$$

$$F_{drag} = \gamma v_x \quad (7)$$

where K_b is the Boltzmann constant, R is a Gaussian random number with a mean of 0 and a standard deviation of 1, T is the ambient temperature of the particle, D is the particle diameter, γ is the viscosity coefficient, Δt is the unit time set to 100 ns, and v_x is the horizontal velocity of the particle.

Each period is composed of the GNBS-80, GNBS-100, and GNBS-120. The captured particles are required to complete three transitions, with each transition time related to the optical gradient force. More intuitively, the depth of the potential well is often inversely proportional to the switching time. Therefore, the switching time must accommodate the transition at the minimum potential well depth. Given the potential well illustrated in Fig. 4 (d), the switching time can be set as a fixed parameter. Fig. 5(a) and (b) demonstrate the variation in the proportion of particles followed within three periods, with switching times set at 2ms and 4ms. Clearly, when the switching time is set to 2ms, the particles are unable to keep pace with the frequency of hotspot transitions, and the hotspot vanishes during the move from the previous hotspot to the current one. When the switching time is extended to 4ms, the majority of particles have sufficient time to complete the transition.



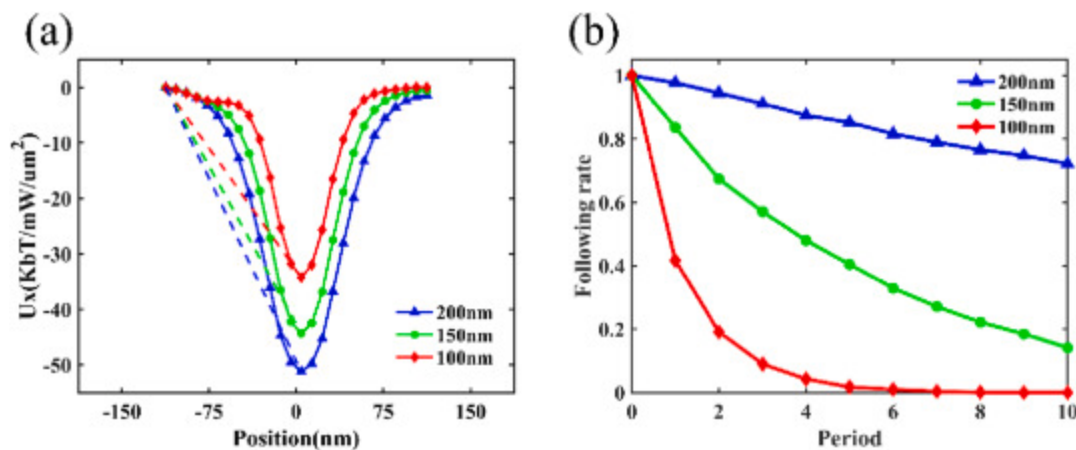
[Download: Download high-res image \(585KB\)](#)

[Download: Download full-size image](#)

Fig. 5. The dashed lines in Fig. 5 (a) and (b) represent the potential well distribution of GNBS-120 on 200nm particles, with the Fermi energy set at 0.88eV. Particle distributions vary over three periods and one period has three switching times when incident light power is $0.4\text{mW}/\mu\text{m}^2$. (a) The switching time is 4ms. (b) The switching time is 2ms.

After completing the analysis of the capture and transfer of particles with a diameter of 200nm, we proceeded to analyze the transfer of particles with two other diameters to verify further whether our designed optical conveyor belt is capable of sorting particles of different diameters. Fig. 6(a) displays the potential well depths for particles of 100nm, 150nm, and 200nm in diameter. The diagonal lines represent the average speed of particles moving towards the hotspot, with a steeper slope indicating faster speed, set at a Fermi energy of 0.67eV. Due to the switching time being set at 4ms, only the 200nm particles achieve sufficient speed to reach the hotspot, while the 100nm and 150nm particles clearly do not have enough speed. Fig. 6(b) illustrates the changes in the following rates with three different diameters over 10 periods. The 200nm particles maintain a following rate of about

72% after 10 periods, while the following rates of the 100nm and 150nm particles rapidly decline to 0% and 14%, respectively, within 10 periods.

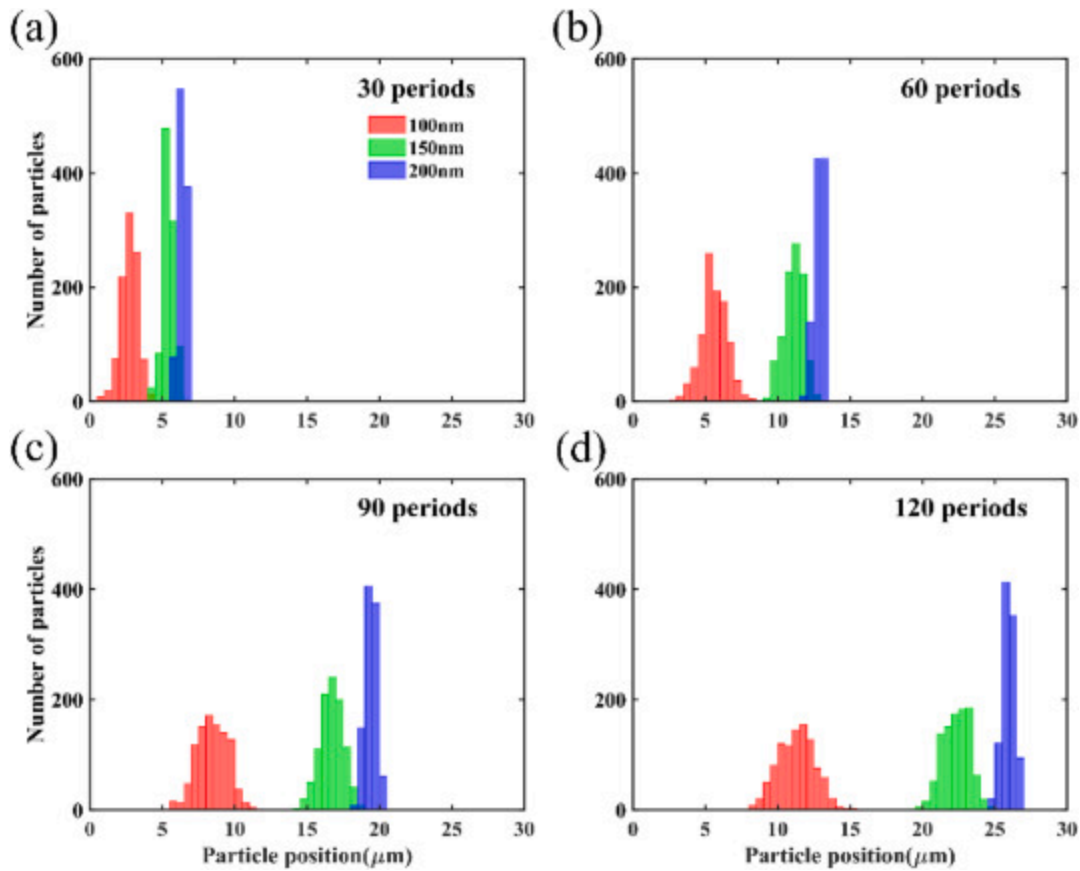


[Download: Download high-res image \(331KB\)](#)

[Download: Download full-size image](#)

Fig. 6. (a) When the Fermi level is set at 0.67eV and the incident light power at $0.4\text{mW}/\mu\text{m}^2$, the GNBS-100 is illuminated to study the potential well distribution in particles with diameters of 100nm, 150nm, and 200nm. (b) Following rates of 100nm, 150nm, and 200nm particles within 10 periods.

Based on Einstein's theory of Brownian motion, we conducted a numerical analysis of particle movement over 120 periods. We released 1000 particles at the starting position, with an incident light power of $0.4\text{mW}/\mu\text{m}^2$ and a switching time of 4ms. After several periods, the particle distribution resembled a normal distribution. The diameter of the particles is positively correlated with the gradient optical force experienced. Since the 200nm particles better matched the excited hotspots, compared to the 100nm and 150nm particles, they received sufficient optical force to drive them and could keep up with the switching frequency of the hotspots. As a result, after several periods, the 100nm and 150nm particles gradually fell behind the 200nm particles. As shown in Fig. 7(a), after 30 periods, particles of three different diameters still overlap significantly. As illustrated in Fig. 7(b), by 60 periods, the 100nm particles are completely lagging behind. Fig. 7(c) and (d) show that the 150nm and 200nm particles achieve separation after 120 periods.



[Download: Download high-res image \(354KB\)](#)

[Download: Download full-size image](#)

Fig. 7. The distributions of particles with diameters of 100nm, 150nm, and 200nm were displayed over periods of 30, 60, 90, and 120, respectively. The switching time is set as 4ms and the power at $0.4\text{mW}/\mu\text{m}^2$.

4. Conclusions

In summary, our proposed optical conveyor belt comprises GNBS-80s, GNBS-100s, and GNBS-120s, designed to capture and sort particles of varying diameters by manipulating the Fermi energy. Initially, it is crucial to analyze the impact of width variations in graphene nano-butterfly structures (GNBSs) on the resonance wavelength and to confirm the capability of GNBSs to capture particles. Subsequently, based on a designed resonance wavelength of $10.6\mu\text{m}$, we determine the specific structural parameters and Fermi levels for the three GNBS sets used in the optical conveyor belt. Further analysis is required on the transfer problem of particles with a diameter of 200nm that have been captured, particularly whether these particles can complete transitions between two plasmonic traps. This involves assessing whether optical forces can propel particles toward hotspots and if they can reach the target position within a designated time. Additionally, for the particle

sorting issue, the distribution of particles with diameters of 100nm, 150nm, and 200nm was evaluated by numerically simulating the motion of 1000 particles over 120 periods.

Funding

This work was supported by the National Natural Science Foundation of China (NSFC)([62105161](#)) and "Taihu Light" Science and Technology Project of Wuxi(No. [K20231036](#)).

Disclosures

The authors declare no conflicts of interest.

Data availability

No data was used for the research described in the article.

CRedit authorship contribution statement

Jinfeng Li: Writing – original draft, Investigation, Formal analysis, Data curation, Conceptualization. **Jinyang Gong:** Formal analysis, Data curation, Conceptualization. **Zhihao Li:** Writing – original draft, Methodology, Conceptualization. **Xiaoling Li:** Funding acquisition, Writing – review & editing. **Min Jiang:** Writing – review & editing, Funding acquisition.

Declaration of competing interest

The authors declare the following financial interests/personal relationships which may be considered as potential competing interests:Min Jiang reports financial support was provided by National Natural Science Foundation of China. Xiaoling Li reports financial support was provided by Wuxi City People's Government. Min Jiang reports a relationship with National NaturalScience Foundation of China that includes: funding grants. If there are other authors, they declare that they have no known competing financial interests or personal relationships that could have appeared to influence the work reported in this paper.

[Recommended articles](#)



Data availability

No data was used for the research described in the article.

References

- [1] A. Ashkin, J.M. Dziedzic, J.E. Bjorkholm, S. Chu
Observation of a single-beam gradient force optical trap for dielectric particles
Opt. Lett., 11 (1986), pp. 288-290
[View in Scopus ↗](#) [Google Scholar ↗](#)
- [2] T.T. Perkins
Optical traps for single molecule biophysics: a primer
Laser Photon. Rev., 3 (2009), pp. 203-220
[Crossref ↗](#) [View in Scopus ↗](#) [Google Scholar ↗](#)
- [3] D.G. Kotsifaki, S. Nic Chormaic
Plasmonic optical tweezers based on nanostructures: fundamentals, advances and prospects
Nanophotonics, 8 (2019), pp. 1227-1245
[Crossref ↗](#) [View in Scopus ↗](#) [Google Scholar ↗](#)
- [4] W. Zhang, L. Huang, C. Santschi, O.J. Martin
Trapping and sensing 10 nm metal nanoparticles using plasmonic dipole antennas
Nano Lett., 10 (2010), pp. 1006-1011
[Crossref ↗](#) [View in Scopus ↗](#) [Google Scholar ↗](#)
- [5] Z. Kang, H. Zhang, H. Lu, J. Xu, H.C. Ong, P. Shum, H.P. Ho
Plasmonic optical trap having very large active volume realized with nano-ring structure
Opt Lett, 37 (2012), pp. 1748-1750
[View in Scopus ↗](#) [Google Scholar ↗](#)
- [6] M. Belkin, S.H. Chao, M.P. Jonsson, C. Dekker, A. Aksimentiev
Plasmonic nanopores for trapping, controlling displacement, and sequencing of DNA
ACS Nano, 9 (2015), pp. 10598-10611
[Crossref ↗](#) [View in Scopus ↗](#) [Google Scholar ↗](#)

- [7] K. Wang, E. Schonbrun, P. Steinvurzel, K.B. Crozier
Scannable plasmonic trapping using a gold stripe
Nano Lett., 10 (2010), pp. 3506-3511
[Crossref ↗](#) [View in Scopus ↗](#) [Google Scholar ↗](#)
- [8] K. Wang, E. Schonbrun, P. Steinvurzel, K.B. Crozier
Trapping and rotating nanoparticles using a plasmonic nano-tweezer with an integrated heat sink
Nat. Commun., 2 (2011), p. 469
[View in Scopus ↗](#) [Google Scholar ↗](#)
- [9] T.D. Bouloumis, D.G. Kotsifaki, S. Nic Chormaic
Enabling self-induced back-action trapping of gold nanoparticles in metamaterial plasmonic tweezers
Nano Lett., 23 (2023), pp. 4723-4731
[Crossref ↗](#) [View in Scopus ↗](#) [Google Scholar ↗](#)
- [10] D.G. Kotsifaki, R. Rajiv Singh, S. Nic Chormaic, V.G. Truong
Asymmetric split-ring plasmonic nanostructures for the optical sensing of Escherichia coli
Biomed. Opt Express, 14 (2023), pp. 4875-4887
[Crossref ↗](#) [View in Scopus ↗](#) [Google Scholar ↗](#)
- [11] S. Tokonami, S. Kurita, R. Yoshikawa, K. Sakurai, T. Suehiro, Y. Yamamoto, M. Tamura, O. Karthaus, T. Iida
Light-induced assembly of living bacteria with honeycomb substrate
Sci. Adv., 6 (2020), Article eaaz5757
[View in Scopus ↗](#) [Google Scholar ↗](#)
- [12] P. Hansen, Y. Zheng, J. Ryan, L. Hesselink
Nano-optical conveyor belt, part I: theory
Nano Lett., 14 (2014), pp. 2965-2970
[Crossref ↗](#) [View in Scopus ↗](#) [Google Scholar ↗](#)
- [13] Y. Zheng, J. Ryan, P. Hansen, Y.T. Cheng, T.J. Lu, L. Hesselink
Nano-optical conveyor belt, part II: demonstration of handoff between near-field optical traps
Nano Lett., 14 (2014), pp. 2971-2976
[Crossref ↗](#) [View in Scopus ↗](#) [Google Scholar ↗](#)

- [14] M. Jiang, G. Wang, W. Xu, W. Ji, N. Zou, H.P. Ho, X. Zhang
Two-dimensional arbitrary nano-manipulation on a plasmonic metasurface
Opt Lett, 43 (2018), pp. 1602-1605
[Crossref ↗](#) [View in Scopus ↗](#) [Google Scholar ↗](#)
- [15] A. Vakil, N. Engheta
Transformation optics using graphene
Science, 332 (2011), pp. 1291-1294
[Crossref ↗](#) [View in Scopus ↗](#) [Google Scholar ↗](#)
- [16] M. Heidari, V. Faramarzi, Z. Sharifi, M. Hashemi, S. Bahadori-Haghighi, B. Janjan, D. Abbott
A high-performance TE modulator/TM-pass polarizer using selective mode shaping in a VO₂-based side-polished fiber
Nanophotonics, 10 (2021), pp. 3451-3463
[Crossref ↗](#) [View in Scopus ↗](#) [Google Scholar ↗](#)
- [17] P. Pinapati, J.P. Joby, S. Cherukulappurath
Graphene oxide based two-dimensional optical tweezers for low power trapping of quantum dots and E. coli bacteria
ACS Appl. Nano Mater., 3 (2020), pp. 5107-5115
[Crossref ↗](#) [View in Scopus ↗](#) [Google Scholar ↗](#)
- [18] Y. Ren, W. Cui, Z. Yang, B. Xiong, L. Zhang, Z. Li, S. Lu, Y. Huo, X. Wu, G. Li, L. Bai, Z. He
Ultra-broadband and wide-angle solar absorber for the All-MXene grating metamaterial
Opt. Mater., 149 (2024), Article 115073
 [View PDF](#) [View article](#) [View in Scopus ↗](#) [Google Scholar ↗](#)
- [19] Y. Wang, W. Cui, Y. Ren, Z. Li, L. Zhang, W. Lei, Y. Huo, Z. He
Tunable perfect absorption and versatile applications based on a simple black phosphorus metasurface in terahertz
Infrared Phys. Technol., 136 (2024), Article 105091
 [View PDF](#) [View article](#) [View in Scopus ↗](#) [Google Scholar ↗](#)
- [20] A.A. Balandin, S. Ghosh, W. Bao, I. Calizo, D. Teweldebrhan, F. Miao, C.N. Lau
Superior thermal conductivity of single-layer graphene
Nano Lett., 8 (2008), pp. 902-907
[Crossref ↗](#) [View in Scopus ↗](#) [Google Scholar ↗](#)
- [21] M.M. Abbasi, S. Darbari, M.K. Moravvej-Farshi

Tunable plasmonic force switch based on graphene nano-ring resonator for nanomanipulation

Opt Express, 27 (2019), pp. 26648-26660

[Crossref ↗](#) [View in Scopus ↗](#) [Google Scholar ↗](#)

- [22] M. Danesh, M.J. Zadeh, T. Zhang, X. Zhang, B. Gu, J.S. Lu, T. Cao, Z. Liu, A.T.S. Wee, M. Qiu, Q. Bao, S. Maier, C.W. Qiu

Monolayer conveyor for stably trapping and transporting sub-1 nm particles

Laser Photon. Rev., 14 (2020), Article 2000030

[View in Scopus ↗](#) [Google Scholar ↗](#)

- [23] P.Q. Liu, P. Paul

Graphene nanoribbon plasmonic conveyor belt network for optical trapping and transportation of nanoparticles

ACS Photonics, 7 (2020), pp. 3456-3466

[Crossref ↗](#) [View in Scopus ↗](#) [Google Scholar ↗](#)

- [24] A.A. Khorami, B. Barahimi, S. Vatani, A.S. Javanmard

Tunable plasmonic tweezers based on graphene nano-taper for nano-bio-particles manipulation: numerical study

Opt Express, 31 (2023), pp. 21063-21077

[Crossref ↗](#) [View in Scopus ↗](#) [Google Scholar ↗](#)

Cited by (0)

© 2024 The Authors. Published by Elsevier B.V.



All content on this site: Copyright © 2024 Elsevier B.V., its licensors, and contributors. All rights are reserved, including those for text and data mining, AI training, and similar technologies. For all open access content, the Creative Commons licensing terms apply.

